Electronic structure of two-dimensional transition metal dichalcogenide bilayers from *ab initio* theory

L. Debbichi,[1,2] O. Eriksson,[2] and S. Lebègue[1]

[1]*Laboratoire de Cristallographie, Résonance Magnétique et Modélisations (CRM2, UMR CNRS 7036) Institut Jean Barriol, Université de Lorraine, BP 239, Boulevard des Aiguillettes 54506 Vandoeuvre-lès-Nancy, France*

[2]*Department of Physics and Astronomy, Box 516, Uppsala University, SE-751 20 Uppsala, Sweden*

(Received 5 March 2014; published 20 May 2014)

By means of first-principles GW calculations, we have studied the electronic structure properties of MX_2 (M = Mo, W; X = S, Se, Te) bilayers, including hybrid structures of MX_2 building blocks. The effect of spin-orbit coupling on the electronic structure and the effect of van der Waals interaction on the geometry were taken into account. All the homogeneous bilayers are identified as indirect band-gap materials, with an increase of the band gap when Mo is changed to W, and a decrease of the band gap when the atomic number of X is increased. The same behavior is also observed for hybrid bilayers with common chalcogen atoms, while bilayers with common metal atoms have a direct band gap. Finally, it is shown that due to their particular band alignment, some heterobilayers enable electron-hole separation, which is of interest for solar cell applications.

DOI: 10.1103/PhysRevB.89.205311 PACS number(s): 31.15.A−, 71.20.Nr, 73.22.−f

I. INTRODUCTION

Since the celebrated discovery of graphene, two-dimensional crystals have been the subject of an intensive research due to their electronic, optical, and mechanical properties [1]. Layered transition-metal dichalcogenides (TMDs) are a class of materials in which layers are stacked together by van der Waals forces [2,3]. They exhibit a large variety of electronic structures such as metallic, semiconducting, or superconducting, depending on the coordination and oxidation states of the metal atom. After it became possible to prepare them in a monolayer or few layers form by the exfoliation technique [4] or by chemical vapor deposition [5], there has been an increasing interest to study the properties of these materials for nanoscale electronics and photonics applications. Several distinctive electronic and optical properties, including a crossover from an indirect gap to a direct gap in the limit of monolayer thickness [6–8], strong excitonic effects [9,10], and the possibility of full optical control of the valley and spin occupation [11,12] have been recently demonstrated for these materials. When increasing the thickness of the MX_2 sheets, they exhibit additional properties not seen in single layers, where the interlayer interaction, geometrical confinement, and crystal symmetry play a collective role in defining their electronic properties [7]. Recently, various basic electronic components have been fabricated based on MoS_2 monolayers and bilayers, such as field-effects transistors (FETs) with a high mobility, sensors, logic circuits, and phototransistors [13–16].

Also, the isolation of various two-dimensional (2D) materials, and the possibility to combine them in vertical stacks has created a new class of van der Waals heterostructures, and has opened the way to the realization of truly 2D-device architectures [17]. Such a concept has already proven to be fruitful for a number of electronic applications in the area of ultrathin and flexible devices with various functionalities [18,19]. For example, stacking TMDs or h-BN over graphene will open a band gap, which allows the fabrication of field effect transistors with very low OFF currents. Also, the construction of 2D heterostructures from a semiconducting layer (MoS_2, WS_2, or GaSe) sandwiched between graphene sheets leads to photovoltaic effects with external quantum efficiencies as high as 30% [20]. Recently, electronic and memory devices have been constructed from the graphene/MoS_2 system and have displayed remarkable optoelectronic functionalities, including highly sensitive photodetection and gate-tunable persistent photoconductivity [21–23]. In addition to FETs, heterojunction diodes have also been constructed using epitaxial growth of a p-WSe_2 layer on top of an n-$MoSe_2$ substrate [24].

At the same time, theoretical studies can be very helpful to understand the properties of stacks of TMD layers, in particular their electronic structure. For instance, calculations at the DFT level (using the GGA approximation) have shown that a MX_2 bilayer undergoes a semiconductor-to-metal transition under uniaxial or biaxial compressive strain [25,26]. The same behavior has also been predicted if an electric field is applied perpendicularly to the layers [27]. In addition, other calculations [28,29] using GGA and HSE have studied how to engineer the band gap of TMDs heterojunctions. However, standard DFT is not able to provide a realistic value of the band gap, and therefore some studies have been conducted using many-body theories. For example, Cheiwchanchamnangij *et al.* [30] have used the GW approximation and the Bethe-Salpether equation to study the optical properties of a MoS_2 bilayer, and a good agreement with absorption experiments was found. Also, Komsa *et al.* [31] have used the same approach to study the effect of quantum confinement on the electronic structure of few MoS_2 layers.

However, these studies have not been generalized to other type of bilayer systems. In particular, the electronic structure properties of MX_2 bilayers (with M being either Mo or W and X = S, Se, or Te), including heterobilayers (also called here hybrid structures), have not been investigated systematically using the GW approximation, which is the purpose of the present publication. Our paper is organized as follows. After a description of the computational details, we will present our results concerning the electronic structure of the homogeneous bilayers, followed by the properties of the heterobilayers. In the last part, we offer our conclusions and perspectives.

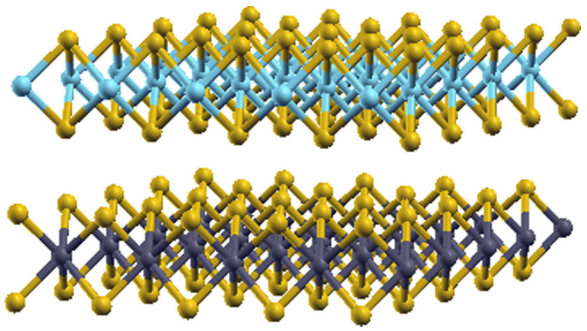

FIG. 1. (Color online) Perspective view of a transition metal dichalcogenide hybrid system stacked in an AB fashion. Transition metal atoms are in blue or gray color and chalcogenide atoms are in yellow.

II. COMPUTATIONAL METHODS

Our first-principles calculations have been performed with the projector-augmented wave (PAW) scheme as implemented in the VASP [32,33] code. The Perdew-Burke-Ernzerhof (PBE) [34] parametrization of the generalized gradient approximation (GGA) is used for the exchange-correlation potentials with a plane-wave cutoff of 400 eV and a $12 \times 12 \times 1$ k-point mesh. The van der Waals interactions are taken into account through a dispersion correction as proposed by Tkatchenko-Scheffler (DFT-TS) [35] and recently implemented in VASP [36]. For a given TMD layer, several polymorphs are known, but only the 2H form was considered here since it is the most stable one according to previous work [37]. Also, the AB stacking, i.e., when the X atoms of one layer are on top of the metal atoms of the other layer, as presented in Fig. 1, was chosen as it is the energetically favored configuration over the AA stacking [26]. Also, only systems with a small lattice mismatch were investigated in our study, which exclude for instance $MoTe_2/MoS_2$ and WTe_2/WS_2 bilayers. The two-dimensional slab geometries were set up with a vacuum space of about 20 Å to ensure decoupling between periodically repeated systems. Then each system was fully relaxed with residual forces smaller than 0.001 eV/Å. These ground-state calculations were then used to compute the quasiparticle band structure with the GW approximation. 352 bands were used in the summation over bands in the calculation of the polarizability and the self-energy and a cutoff of 150 eV was used for the size of the polarizability matrices. Also, 100 frequency points were used for the integration over frequency in the calculation of the self-energy. The spin-orbit interaction was included both at the DFT and GW levels.

III. RESULTS AND DISCUSSION

The list of investigated MX_2 bilayer systems, their structural parameters, and their calculated quasiparticle band gap are presented in Tables I and II, together with the available experimental data. As shown in Table I, the calculated lattice parameters of the homogeneous structures are in good agreement with the experimental values of the corresponding bulk systems, and the interlayer distances (measured as the chalcogen-chalcogen distance along the stacking direction) differ only slightly from the experimental data. These two parameters are compared to the bulk values due to absence of experimental data for the bilayers. The results are also in good agreement with previous calculations on bulk MoS_2 using the same method [36]. Our calculated quasiparticle band gaps are reported in Table I along with the measured photoluminescence gap [7] for the MoS_2 bilayer. For MoS_2, the GW band gap is found to be larger by ∼0.2 eV in comparison with the experimental value and in good agreement with the previous calculations [30,31]. This overestimation is mainly due to excitonic effects [30], which are not included at the GW level of theory. According to our calculations, all the MX_2 bilayers present indirect band gaps, in contrast to the direct gap of the corresponding monolayers. For a given X, the band gap of a WX_2 compound is slightly larger than the band gap of the corresponding MX_2 compound, and the magnitude of the band gap decreases when going from sulphide to the telluride due to the decrease in ionicity.

Without including spin-orbit coupling in the calculation, all the homogeneous bilayers have an indirect band gap with the valence-band maxima (VBM) located at Γ and the conduction-band minima (CBM) at Λ (along the Γ-K direction, data not shown). Due to the interlayer hopping, the valence bands are splitted in two groups of double degenerated bands. Also, the interlayer interaction acts more at Γ than at K due to the different localisation of the wave function at these points [39]. As the chalcogen atom changes from S, Se, to Te the magnitude of the splitting increases due to the increased interlayer coupling [40]. However, when SO coupling is included, the band structures are modified (see

TABLE I. In plane lattice parameters a, interlayer distances d (in Å), and quasiparticle band gaps (in eV) of homogeneous MX_2 bilayers. For comparison, the experimental (exp) values for the geometry of the corresponding bulk crystal are also presented. Δ_{sp} is the splitting at the valence band maximum at the K point.

Bilayers	a_{cal}	a_{exp}	d	d_{exp} [38]	Δ_{sp}	$E_g^{G_0W_0+soc}$	E_g^{exp}
MoS_2	3.16	3.16	2.92	2.98	0.18	1.83 (Γ-Λ)	1.6 [7]
$MoSe_2$	3.29	3.30	3.06	3.07	0.21	1.67 (Γ-Λ)	
$MoTe_2$	3.52	3.52	3.38	3.49	0.24	1.32 (K-Λ)	
WS_2	3.17	3.15	3.01	3.02	0.40	2.06 (Γ-Λ)	
WSe_2	3.29	3.28	3.14	3.14	0.47	1.76 (K-Λ)	
WTe_2	3.52	3.52	3.45	–	0.49	1.33 (K-Λ)	

TABLE II. Calculated lattice parameters a, interlayers distances d, and quasiparticle band gaps E_g of TMDs heterobilayers using GGA and G_0W_0 with SO coupling. Δ_{so} is the value of the spin orbit splitting at the top of the valence bands.

Bilayers	a_{cal}	d	Δ_{so}	$E_g^{G_0W_0+soc}$
WS_2-MoS_2	3.16	2.97	0.32	1.96 (Γ-Λ)
WSe_2-$MoSe_2$	3.29	3.10	0.30	1.67 (K-Λ)
WTe_2-$MoTe_2$	3.49	3.42	0.26	1.31 (K-Λ)
$MoSe_2$-MoS_2	3.22	2.99	0.17	1.25 (K-K)
$MoTe_2$-$MoSe_2$	3.40	3.19	0.20	1.13 (K-K)
WSe_2-WS_2	3.23	3.08	0.41	1.26 (K-K)
WTe_2-WSe_2	3.40	3.28	0.40	1.12 (K-K)

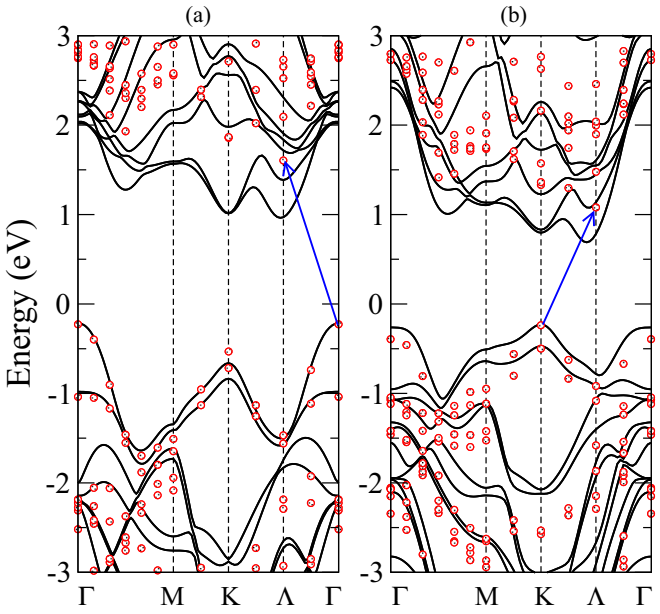

FIG. 2. (Color online) Band structure of MoS_2 (a) and $MoTe_2$ (b) bilayers: black lines and red dots represent the GGA and G_0W_0 calculation with SO coupling, respectively. The Fermi level is put to zero, the band gap is indicated by an arrow and the vertical lines indicate the positions of high-symmetry points.

Fig. 2 for MoS_2 and $MoTe_2$ bilayer band structures), with a downshift of the lowest conduction band along K-Γ by ∼50 meV and an upshift of the valence band maximum at the K point. As a result, the energy band gap of $MoTe_2$, WSe_2, and WTe_2 bilayer changes from Γ-Λ to K-Λ.

The band splitting Δ_{sp} at the top of the valence bands at the K point of the considered homogeneous bilayers are reported in Table I. The value of Δ_{sp} in the bilayer is due to both SO and interlayer couplings. As shown in Table I Δ_{sp} lies in the range ∼0.2–0.49 eV depending on the size of the TM atom. The calculated Δ_{sp} are in good agreement with the splitting observed in the photoluminescence spectra of a MoS_2 bilayer with a magnitude of ∼0.2 eV [7] and of WS_2 and WSe_2 bilayers with a magnitude of ∼0.4 eV [41].

Turning now to heterobilayers (see Table II), we have distinguished two groups: the first group is with common chalcogen atoms (called X-common bilayers), and the second group is with common TM atoms (called M-common bilayers). For common chalcogen atoms, the in-plane lattice constant of the MX_2 monolayers are very close to each others, while they differ slightly more for common TM atoms. Also, the lattice parameters and interlayer distances of M-common heterobilayers are almost equal to the average of the homogeneous bilayers values. For X-common heterobilayers, the interlayer distances correspond to a value close to the average of the corresponding homogeneous bilayers. Also, all the X-common systems studied here present an excellent in plane lattice matching, indicating that they can be used for building heterojunction diodes [26].

As shown in Table II, the bilayers of the X-common group have an indirect band gap, which gradually decreases as the atomic number of the chalcogen atom increases, similar to

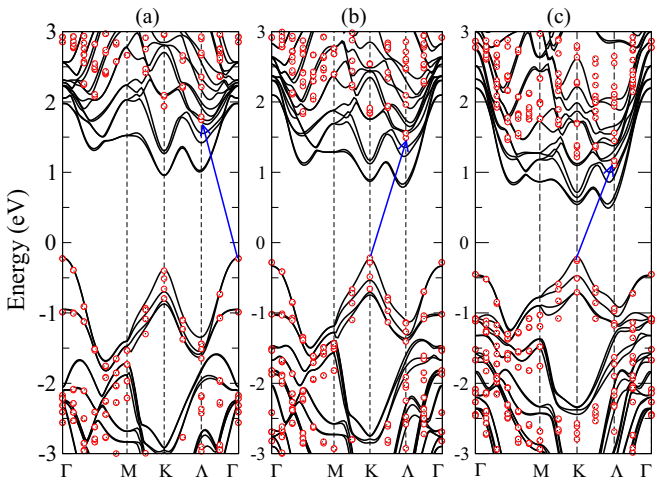

FIG. 3. (Color online) Band structure of WS_2-MoS_2 (a), WSe_2-$MoSe_2$ (b), WTe_2-$MoTe_2$ (c) heterobilayers: black lines and red dots represent GGA and G_0W_0 calculation with SO coupling, respectively. The Fermi level is put to zero, and band gap is indicated by an arrow. The vertical lines indicate the positions of high-symmetry points.

what is observed for single layers. Without SO coupling (data not shown), the band gap remains indirect with a VBM located at Γ and a CBM located at Λ. However, when SO-coupling is included, the degenerated valence bands are splitted into nondegenerated states around the K point, a behavior which is observed for all the considered heterobilayers. Then, the VBM of the $MoSe_2$-WSe_2 and the $MoTe_2$-WTe_2 bilayers are changed from Γ to K while the CBM remains at Λ. As seen in Fig. 3, the DFT and G_0W_0 band structures differ for the MoS_2-WS_2 bilayer, since DFT gives a CBM located at K while the GW approximation puts it at Λ.

M-common heterostructures have a direct band gap at the K point (see Fig. 4) with a value obtained with the GW

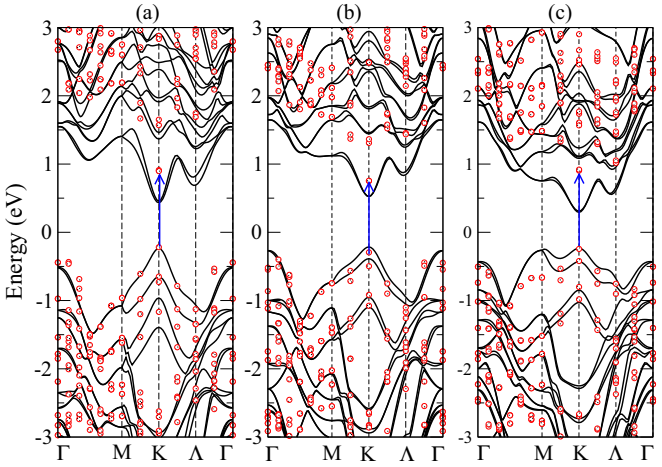

FIG. 4. (Color online) Band structure of WSe_2-WS_2 (a), $MoSe_2$-MoS_2 (b), $MoTe_2$-$MoSe_2$ (c) heterobilayers: black lines and red dots represent GGA and G_0W_0 calculations with SO coupling, respectively. The Fermi level is put to zero, and band gap is indicated by an arrow. The vertical lines indicate the positions of high-symmetry points.

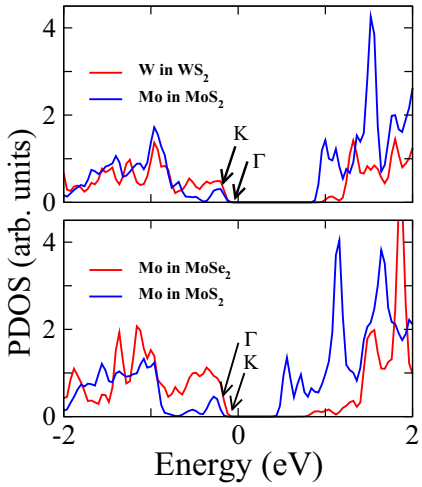

FIG. 5. (Color online) Partial densities of states of WS_2-MoS_2 (top), $MoSe_2$-MoS_2 (bottom), showing type-II alignment.

approximation in the range ∼1.1–1.3 eV (see Table II). For some M-common bilayers, a direct band gap is observed only when the SO coupling interaction is taken into account: without SO coupling (data not shown), $MoSe_2$-MoS_2 and $MoTe_2$-$MoSe_2$ bilayers have an indirect bandgap from Γ to K and from M to K, respectively, whereas the WSe_2-WS_2 and WTe_2-WSe_2 heterostructures exhibit a direct band gap with or without SO coupling. Similarly to MX_2 single layers, the splitting at the top of the VBM of the MX_2 heterobilayers comes from SO coupling as a result of the missing inversion symmetry [42]. The value of Δ_{so} (the splitting at the VBM) is reported in Table II for all the heterobilayers studied here. For X-common bilayers, the value of Δ_{so} increases when going from S to Te due to the decreasing distances between the chalcogen atoms, while for M-common bilayers, Δ_{so} increases with increasing the TM atomic number.

According to our calculated density of states, the top of the VBM and the bottom of the CBM belong to different layers, as shown for example in Fig. 5 for the WS_2-MoS_2 and the $MoSe_2$-MoS_2 heterobilayers. In both cases, we find that the MoS_2 monolayer behaves as the electron acceptor and the other layer acts as the electron donor, which is in agreement with previous discussions [43,44] on the band alignment of MX_2 monolayers. This is further proven by looking at the charge density at the K point (which corresponds to the minimum direct gap) for the VBM and the CBM. As seen in Fig. 6 for the WS_2-MoS_2 and the $MoSe_2$-MoS_2 bilayers, the charge density at the CBM state is found to be mainly localized on the MoS_2 monolayer (around the Mo atoms), while the VBM state belongs to the second monolayer and is more uniformly distributed among the atoms.

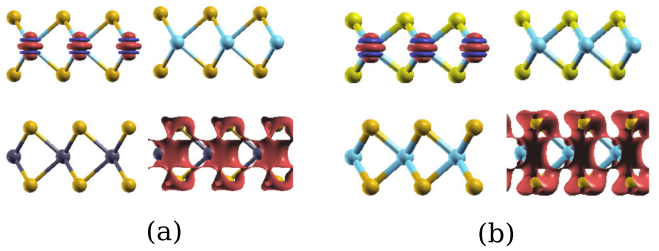

FIG. 6. (Color online) Charge separation at the interface of WS_2-MoS_2 (a) and $MoSe_2$-MoS_2 (b) heterobilayers. For each figure, the left part corresponds to the top of the highest valence band at the K point and the right part corresponds to the bottom of the lowest conduction band at the K point.

This particular electronic structure, with the valence-band maximum belonging to one layer and the conduction-band minimum belonging to an other layer allows, in principle, an efficient electron-hole separation, which is crucial for solar cell applications [45]. This was shown previously for the case of WS_2-MoS_2 [46] but according to our calculations, the same mechanism is expected to happen with all the heterobilayers studied here, except the WSe_2-WTe_2 in which the electrons and holes are localized on the same layer.

IV. SUMMARY

In summary, we have performed first-principles GW calculations to study the electronic structure of MX_2 bilayers (with M being either Mo or W and X = S, Se, or Te), including heterobilayers. In all our calculations, van der Waals interaction and spin-orbit coupling were included in order to get accurate results. All the homogeneous bilayers are identified as indirect band-gap semiconductors. In the case of heterobilayers, X-common bilayers have an indirect band gap whereas the M-common bilayers have a direct band gap. For both homo- and heterobilayers, the band gap depends significantly on the atomic species, and when Mo changed to W the band gap is increased, while when the atomic number of X increases, the band gap decreased. Also, due to the band alignment, the MX_2 heterobilayers can be potentially used as charge separators for solar-cell applications.

ACKNOWLEDGMENTS

The authors acknowledge DARPA and Navy-NICOP for funding. O.E. gratefully acknowledges the European Research Council (ERC Project No. 247062), the Swedish Research Council (VR), SSF, and the Knut and Alice Wallenberg Foundation for financial support. O.E. also acknowledges eSSENCE and STANDUPP. This work was performed using HPC resources from GENCI-CCRT/CINES (Grant x2014-085106).

[1] S. Z. Butler, S. M. Hollen, L. Cao, Y. Cui, J. A. Gupta, H. R. Gutierrez, T. F. Heinz, S. S. Hong, J. Huang, A. F. Ismach, E. Johnston-Halperin, M. Kuno, V. V. Plashnitsa, R. D. Robinson, R. S. Ruoff, S. Salahuddin, J. Shan, Li Shi, M. G. Spencer, M. Terrones, W. Windl, and J. E. Goldberger, ACS Nano **7**, 2898 (2013).

[2] J. A. Wilson and A. D. Yoffe, Adv. Phys. **18**, 193 (1969).
[3] A. Enyashin, S. Gemming, and G. Seifert, Eur. Phys. J. Spec. Top. **149**, 103 (2007).
[4] K. S. Novoselov, D. Jiang, F. Schedin, T. J. Booth, V. V. Khotkevich, S. V. Morozov, and A. K. Geim, Proc. Natl. Acad. Sci. U.S.A. **102**, 10451 (2005).
[5] S. Balendhran, J. Z. Ou, M. Bhaskaran, S. Sriram, S. Ippolito, Z. Vasic, E. Kats, S. Bhargava, S. Zhuiykov, and K. Kalantar-zadeh, Nanoscale **4**, 461 (2012).
[6] A. Splendiani, L. Sun, Y. Zhang, T. Li, J. Kim, C.-Y. Chim, and F. Wang, Nano Lett **10**, 1271 (2010).
[7] K. F. Mak, C. Lee, J. Hone, J. Shan, and T. F. Heinz, Phys. Rev. Lett. **105**, 136805 (2010).
[8] S. Lebègue and O. Eriksson, Phys. Rev. B **79**, 115409 (2009).
[9] K. F. Mak, K. He, C. Lee, G. H. Lee, J. Hone, T. F. Heinz, and J. Shan, Nat. Mater **12**, 207 (2013).
[10] J. S. Ross, S. Wu, H. Yu, N. J. Ghimire, A. M. Jones, G. Aivazian, J. Yan, D. G. Mandrus, D. Xiao, W. Yao, and X. Xu, Nat. Commun **4**, 1474 (2013).
[11] D. Xiao, G.-B. Liu, W. Feng, X. Xu, and W. Yao, Phy. Rev. Lett. **108**, 196802 (2012).
[12] S. Wu, J. S. Ross, G.-B. Liu, G. Aivazian, A. Jones, Z. Fei, W. Zhu, D. Xiao, W. Yao, D. Cobden, and X. Xu, Nat. Phys. **9**, 149 (2013).
[13] B. Radisavljevic, M. B. Whitwick, and A. Kis, ACS Nano **5**, 9934 (2011).
[14] B. Radisavljevic, A. Radenovic, J. Brivio, V. Giacometti, and A. Kis, Nat. Nanotechnol. **6**, 147 (2011).
[15] Z. Yin, H. Li, H. Li, L. Jiang, Y. Shi, Y. Sun, G. Lu, Q. Zhang, X. Chen, and H. Zhang, ACS Nano **6**, 74 (2012).
[16] H. Wang, L. L. Yu, Y. H. Lee, Y. M. Shi, A. Hsu, M. L. Chin, L. J. Li, M. Dubey, J. Kong, and T. Palacios, Nano Lett. **12**, 4674 (2012).
[17] A. K. Geim and I. V. Grigorieva, Nature (London) **499**, 419 (2013)
[18] A. S. Mayorov, R. V. Gorbachev, S. V. Morozov, L. Britnell, R. Jalil, L. A. Ponomarenko, P. Blake, K. S. Novoselov, K. Watanabe, T. Taniguchi, and A. K. Geim, Nano Lett. **11**, 2396 (2011).
[19] M. Osada and T. Sasaki, Adv. Mater. **24**, 210 (2012).
[20] L. Britnell, R. M. Ribeiro, A. Eckmann, R. Jalil, B. D. Belle, A. Mishchenko, Y.-J. Kim, R. V. Gorbachev, T. Georgiou, S. V. Morozov, A. N. Grigorenko, A. K. Geim, C. Casiraghi, A. H. Castro Neto, and K. S. Novoselov, Science **340**, 1311 (2013).
[21] S. Bertolazzi, D. Krasnozhon, and A. Kis, ACS Nano **7**, 3246 (2013).
[22] M. S. Choi, G. H. Lee, Y. J. Yu, D. Y. Lee, S. H. Lee, P. Kim, J. Hone, and W. J. Yoo, Nat. Commun. **4**, 1624 (2013).
[23] K. Roy, M. Padmanabhan, S. Goswami, T. P. Sai, G. Ramalingam, S. Raghavan, and A. Ghosh, Nat. Nanotechnol. **8**, 826 (2013).
[24] R. Spah, M. Luxsteiner, M. Obergfell, E. Bucher, and S. Wagner, Appl. Phys. Lett. 1985 **47**, 871 (1985).
[25] E. Scalise, M. Houssa, G. Pourtois, V. Afanasev, and A. Stesmans, Nano Res. **5**, 43 (2012).
[26] S. Bhattacharyya and A. K. Singh, Phys. Rev. B **86**, 075454 (2012).
[27] A. Ramasubramaniam, D. Naveh, and E. Towe, Phys. Rev. B **84**, 205325 (2011).
[28] K. Kośmider and J. Fernández-Rossier, Phys. Rev. B **87**, 075451 (2013).
[29] H. Terrones, F. Lopez-Uras, and M. Terrones, Sci. Rep. **3**, 1549 (2013).
[30] T. Cheiwchanchamnangij and W. R. L. Lambrecht, Phys. Rev. B **85**, 205302 (2012).
[31] H.-P. Komsa and A. V. Krasheninnikov, Phys. Rev. B **86**, 241201(R) (2012).
[32] G. Kresse and D. Joubert, Phys. Rev. B **59**, 1758 (1999).
[33] G. Kresse and J. Hafner, Phys. Rev. B **47**, 558 (1993).
[34] J. P. Perdew, K. Burke, and M. Ernzerhof, Phys. Rev. Lett. **77**, 3865 (1996).
[35] A. Tkatchenko and M. Scheffler, Phys. Rev. Lett. **102**, 073005 (2009).
[36] T. Bučko, S. Lebègue, J. Hafner, and J. G. Ángyán, Phys. Rev. B **87**, 064110 (2013).
[37] C. Ataca, H. Sahin, and S. Ciraci, J. Phys. Chem. C **116**, 8983 (2012).
[38] M. A. Py and R. R. Haering, Can. J. Phys. **61**, 76 (1983).
[39] H.-P. Komsa and A. V. Krasheninnikov, Phys. Rev. B **88**, 085318 (2013).
[40] Z. Gong, G.-B. Liu, H. Yu, D. Xiao, X. Cui, X. Xu, and W. Yao, Nat. Commun. **4**, 2053 (2013).
[41] H. Zeng, G.-B. Liu, J. Dai, Y. Yan, B. Zhu, R. He, L. Xie, S. Xu, X. Chen, W. Yao, and X. Cui, Sci. Rep. **3**, 1608 (2013).
[42] Z. Y. Zhu, Y. C. Cheng, and U. Schwingenschlögl, Phys. Rev. B **84**, 153402 (2011).
[43] J. Kang, S. Tongay, J. Zhou, J. Li, and J. Wu, Appl. Phys. Lett **102**, 012111 (2013).
[44] Y. Liang, S. Huang, R. Soklaski, and L. Yang, Appl. Phys. Lett **103**, 042106 (2013).
[45] B. A. Gregg, MRS Bull. **30**, 20 (2005).
[46] M. Bernardi, M. Palummo, and J. C. Grossman, Nano Lett. **13**, 3664 (2013).